Mineralogia, vol. 54, 2023, 58-68 *Original Paper*

DOI: 10.2478/mipo-2023-0006

New synthetic [LREE (LREE = La, Ce, Pr, Sm), Pb]-phosphate phases

Kacper Staszel[1]*, Anna Jędras[1], Mateusz Skalny[1], Klaudia Dziewiątka[1], Kamil Urbański[1], Julia Sordyl[1,2], Karolina Rybka[1,3], Maciej Manecki[1]

[1]AGH University of Kraków; Faculty of Geology, Geophysics and Environmental Protection; Department of Mineralogy, Petrography and Geochemistry, al. Mickiewicza 30, 30-059 Kraków, Poland
[2]Department of Earth Sciences, Uppsala University, Villavägen 16, SE-752 36 Uppsala, Sweden
[3]Institute of Geological Sciences, Polish Academy of Sciences, Senacka 1, 31-002 Kraków, Poland

*Corresponding author: kstaszel@agh.edu.pl

Abstract

Search for inexpensive and efficient methods of critical raw materials recovery is of great importance across the world due to growing demand for green technologies. Formation and detailed characterization of new Pb- and Light Rare Earth Elements (LREE)-containing phosphates, compared to already described Pb- or LREE-containing phosphates, was described in this work. These phases were precipitated at experimental conditions similar to these used in a newly proposed coprecipitation route for REE recovery from aqueous solutions. The formation of La, Ce, Pr and Sm phosphates from aqueous solutions proceeded differently in the presence of Pb than in its absence. No rhabdophane group minerals, $(REE,Ca,Th)(PO_4)\cdot nH_2O$ were formed, which were the product of crystallization in the absence of Pb, as evidenced by the PXRD analysis of the control LREE phosphates. Instead, a new, distinct phase was formed, which is neither a 'phosphoschultenite', $PbHPO_4$, with La, Ce, Pr or Sm substitution nor a rhabdophane with Pb substitution. This showed that $PbHPO_4$ structure did not accept isomorphic substitutions of LREE elements and rhabdophane structures are reluctant to accept Pb substitutions. At the same time, the formation of a hitherto unknown crystalline phase was found to be a mixed (LREE,Pb)-phosphate. A lower pH caused higher crystallinity of phases, as confirmed by SEM and PXRD. FTIR spectroscopy showed the hydrous nature of the obtained phases, which was additionally confirmed by thermal analysis. Decreasing pH of the reaction solution resulted in a higher crystalline water content. Moreover, La-bearing phases contained more chemically bound water than other phases. A combined EDS analysis and ICP-OES led to the chemical composition of new Pb phases with La, Ce, Pr and Sm that can be expressed as $La_2Pb_3(PO_4)_4\cdot 3.5H_2O$, $Ce_2Pb_3(PO_4)_4\cdot 3.3H_2O$, $Pr_2Pb_3(PO_4)_4\cdot 3.1H_2O$ and $Sm_2Pb_3(PO_4)_4\cdot 3.3H_2O$, respectively. These results give a better understanding of potential novel recovery pathways of REE from phosphate mineral sources or wastes.

Keywords: REE phosphates, lead phosphates, rhabdophane, 'phosphoschultenite', monazite

1. Introduction

With the constant improvement of the technological level the potential of rare earth elements (REE) (lanthanides, scandium and yttrium) in a wide variety of fields is continuously being explored. During the last three decades REE have become crucial components in many high and green technologies (Binnemans et al., 2013; Apergis & Apergis, 2017; Balaram, 2019; Proelss et al., 2020). REE are essential not only for an

© Staszel et al. 2023. This work is distributed under the Creative Commons Attribution 4.0 License (http://creativecommons.org/licenses/by/4.0/)

assortment of consumer products like mobile phones, hybrid and electric cars, optical elements, and hard disk drives but they are also indispensable in industrial applications. Wind energy turbines, photovoltaic cells, hydrogen purification systems, optical fibers, and high-performance magnets are only a few examples of wide-ranging industrial appliances of REE (Balaram, 2019; Müller et al., 2016; Proelss et al., 2020). Their relative scarcity, lack of proper substitutes, and China's near-monopoly of the market increase the demand for inexpensive, efficient methods of recovery (Alonso et al., 2012; Mancheri et al., 2019; Müller et al., 2016; Zhang et al., 2022). Many advanced approaches and techniques for the separation of REE have been already developed, although most of them are inefficient and generate a great amount of hazardous waste (He et al., 2019). REE industry produces annually over 20 million tons of wastewater containing a high concentration of ammonia nitrogen (Traore et al., 2022). The most studied methods of REE recovery from solutions include precipitation methods (Li et al., 2022; Vaziri Hassas et al., 2023), chromatographic methods (Kifle & Wibetoe, 2013; Max-Hansen et al., 2011), solid-phase extraction (Pyrzynska et al., 2016; Talan & Huang, 2022), supercritical fluid extraction (Das et al., 2018; Shimizu et al., 2005), ion exchange resins (Ang et al., 2017; Hermassi et al., 2021), and electrochemical methods (Kumari et al., 2021; Makarova et al., 2020).

As Europe and other countries heavily depend on external supplies, there is a growing demand for alternative REE sources (Cánovas et al., 2017). There are attempts to cover for this demand with secondary sources, such as End-of-Life products with a high content of REE. This is particularly important for countries lacking primary deposits. Urban mining of lamps and magnets has been already broadly studied (Belardi et al., 2014; Binnemans et al., 2013; Innocenzi et al., 2014; Laatikainen et al., 2021), nonetheless REE recovery from industrial landfilled stocks has not been sufficiently researched. Phosphogypsum, as an undesirable by-product of the manufacture of phosphate fertilizers, has a particular potential. The amount of phosphogypsum waste is constantly growing, thus the necessity of their storage and disposal generates huge worldwide environmental troubles such as water and soil pollution (Cánovas et al., 2017, 2019; Kulczycka et al., 2016). Phosphogypsum, which is mostly composed of $CaSO_4 \cdot 2H_2O$, often contains unreacted phosphate rocks, gangue mineral particles (e.g., quartz, feldspar, phosphates), and other solid phases, like alkali fluorosilicates and fluorides. Around 70-85% of REE initially present in phosphate rocks are deposited in phosphogypsum and are wasted due to the insufficient, expensive approaches of REE separation (Binnemans et al., 2015; Cánovas et al., 2019; Kulczycka et al., 2016; Rychkov et al., 2018). Therefore, feverish work is underway on technologies for beneficiation of REE from solutions through processing, synthesizing, and using REE-phosphates (Emsbo et al., 2015; Kulczycka et al., 2016).

The general formula of REE-phosphate minerals may be given as $REEPO_4 \cdot nH_2O$. Depending on their hydration content as well as the REE incorporated, they can be divided into four individual structural types — monazite, rhabdophane, churchite, and xenotime (Achary et al., 2017; Clavier et al., 2018). Monazite, which crystalizes in the $P2_1/n$ space group, is an anhydrous compound. The structure of xenotime (typically anhydrous phosphate forming in igneous and metamorphic rocks at high temperatures, synthetic analogs might contain water molecules in [001] channel (Strzelecki et al., 2022)) is hexagonal: it crystallizes in the zircon structure type ($ZrSiO_4$, $I4_1/amd$). The stabilization of these two phases is directly related to the nature of REE integrated into their structure (Gausse et al., 2016). The monazite structure has been recognized only for the light REE (from La to Eu), whereas the xenotime type can be formed just for compounds containing heavier REE (from Ho to Lu and Sc, Y, Dy, Gd, Tb) (Diaz-Guillén et al., 2007; Gausse et al., 2016). Furthermore, the literature depicts hydrated forms of REE-phosphates: churchite– and rhabdophane–group members. The first one, with the general formula $REEPO_4 \cdot 2H_2O$, can be formed with Y and elements from Gd to Lu. It crystalizes in the $C2/c$ space group (Rafiuddin et al., 2022; Subramani et al., 2019). The general formula of rhabdophane may be given as $REEPO_4 \cdot nH_2O$ ($0.5 \leq n \leq 1$). This monoclinic structure belongs to the $C2$ space group and can be formed with elements from La to Dy (Diaz-Guillén et al., 2007; Mesbah et al., 2014, 2017). Hydrated forms of REE-phosphates are far less abundant in nature. Rhabdophane–group members are considered metastable regarding monazite and its occurrence is frequently restricted to the uppermost section of the crust (Gausse et al., 2016). Rhabdophane–group representatives are one of the major carriers of LREE in bauxites and laterites, though monazite is dominant in igneous and metamorphic rocks (Berger et al., 2008). Owing to a variety of prospective applications as geochronometers (Gelcich et al., 2005), phosphor light emitters (Shinde & Dhoble, 2014), thermal barrier coatings (Hossain et al., 2022), or the transmutation of nuclear waste (Sengupta, 2012), the hydrated REE phosphates are intensely studied.

Since Pb and LREE readily form phosphates that precipitate from aqueous solutions, it has been hypothesized that the precipitation of LREE-phosphates in the presence of Pb can lead to the formation of mixed phosphate phases containing both Pb and LREE (such as natural phase UM2006-35-PO:HPbREEY reported by Plasil et al. (2009)). The formation of such mixed phases may be of great technological importance in the future due to emerging new methods of REE beneficiation using Pb phosphates. In this paper, La-Pb, Ce-Pb, Pr-Pb and Sm-Pb phosphate phases were synthesized by precipitation from aqueous solutions at ambient temperature. The effect of Pb on REE in phosphates was studied at various pH. The conditions of the experiments were similar to those used in recently proposed technology for REE removal from solutions by precipitation with Pb phosphates (Sordyl et al., 2023).

The morphology, chemistry, and thermal behavior of obtained materials were also studied. Characterization of new (REE,Pb)-phosphates provide significant knowledge contributing to the development of REE recovery technologies from minerals and waste.

2. Synthesis

(LREE,Pb)-phosphates (where LREE = La, Ce, Pr and Sm) were synthesized at different pH conditions by precipitation from aqueous solutions at ambient temperature (around 21°C) and under atmospheric pressure. Control samples consisted of LREE-phosphates precipitated in the absence of Pb, and Pb phosphate synthesized in the absence of LREE.

The following chemicals were used in the synthesis: $Sm(NO_3)_3 \cdot 6H_2O$ (Acros, purity >99,99%), $La(NO_3)_3 \cdot 6H_2O$ (Acros, purity >99,99%), $Ce(NO_3)_3 \cdot 6H_2O$ (Acros, purity 99,5%), $Pr(NO_3)_3 \cdot 6H_2O$ (Acros, purity 99,9%), $Pb(NO_3)_2$ (Avantor, p.a.), NaH_2PO_4 (Avantor, p.a.), NaOH (Avantor, p.a.), HNO_3 (Avantor, p.a.). Redistilled water was used during the experiments.

A composition of solutions used for synthesis and abbreviations for obtained phases is given in Table 1. Solution 1 contained NaH_2PO_4 dissolved in 50 mL of redistilled water and Solution 2 was composed of a given amount of $La(NO_3)_3 \cdot 6H_2O$, $Ce(NO_3)_3 \cdot 6H_2O$, $Pr(NO_3)_3 \cdot 6H_2O$ or $Sm(NO_3)_3 \cdot 6H_2O$ dissolved in 50 mL of redistilled water. For the synthesis of materials containing lead (LaPb-P, CePb-P, PrPb-P and SmPb-P), a $Pb(NO_3)_2$ was added to Solution 2. The precipitates were obtained by dropwise, simultaneous addition of Solutions 1 and 2 (peristaltic pump, 5 mL/min) into a beaker partially filled with 25 mL of redistilled water. Samples containing La and Sm were synthesized at various pH: 2, 3, and 4 to verify previous observations indicating the effect of pH on crystallinity (Sordyl et al., 2022). The pH was maintained throughout the experiments using a 0.1 M solution of NaOH or HNO_3. After synthesis, the precipitate was centrifuged, washed with redistilled water, and dried at 60°C in an electrical oven for approximately 24 hours. All synthesis procedures resulted in obtaining approximately 0.1 – 1.1 and 1.0 – 1.5 grams of solids, for Pb-free and Pb-containing phases respectively. Significant increase in synthesis yield was observed for Pb-free phases in the function of growing pH.

Table 1. Composition of the solutions used for the syntheses.

Phase	*Solution 1*	*Solution 2*				
	PO_4^{3-} [mol/L]	Sm^{3+} [mol/L]	La^{3+} [mol/L]	Ce^{3+} [mol/L]	Pr^{3+} [mol/L]	Pb^{2+} [mol/L]
La-P	0.045	–	0.045	–	–	–
LaPb-P	0.045	–	0.045	–	–	0.045
Sm-P	0.044	0.044	–	–	–	–
SmPb-P	0.044	0.044	–	–	–	0.044
Ce-P	0.320	–	–	0.320	–	–
CePb-P	0.320	–	–	0.320	–	0.320
Pr-P	0.320	–	–	–	0.320	–
PrPb-P	0.320	–	–	–	0.320	0.320
Pb-P	0.044	–	–	–	–	0.044

3. Solids characterization

To investigate the morphology of the obtained materials scanning electron microscopy (SEM) observations were conducted using FEI Quanta 200 FEG SEM equipped with secondary and backscattered electrons detectors. Chemical composition was estimated by Energy dispersive spectrometry (EDS, FEI Quanta). For wet chemical analysis, precipitates were dissolved in 30% HNO_3 solution and analysed by inductively coupled plasma optical emission spectroscopy (ICP-OES). Powder X-ray diffraction (PXRD) patterns were recorded using a Rigaku SmartLab diffractometer in the range of 2θ = 2–100° with a step size of 0.02, 2 sec/step, using graphite-monochromatized Cu Kα radiation. Program GSAS-II was used for Rietveld modelling and indexing of selected PXRD patterns. Fourier-transform infrared (FTIR) spectra were recorded with a Nicolet 7600 spectrometer in the mid-infrared region (4000 to 400 cm^{-1}). Samples were ground in a mortar with KBr (1 mg of sample with 200 mg KBr). The differential thermal (DTA/TG) analysis of was carried out using Netzsch STA 449F3 instrument coupled with a Quadrupole Mass Spectrometer for gas analysis (Netzsch QMS 403).

4. Results and Discussion

4.1. Phase composition

Comparison of the patterns and identification of synthesis products based on PXRD is shown in Figs. 1 and 2. Control synthesis from solutions containing only Pb and PO_4 ions resulted in precipitation of $PbHPO_4$. This is a synthetic analogue of 'phosphoschultenite' (ICDD card No 06-0274). The name of the phase, proposed by Młynarska et al. (2014) and Wudarska et al. (2022) is not yet approved by IMA. The other control synthesis from solutions containing only LREE and PO_4 ions resulted in precipitation of hydrated phosphates with a monoclinic, rhabdophane structure: $LaPO_4 \cdot 0.66H_2O$, $CePO_4 \cdot 0.66H_2O$, $PrPO_4 \cdot 0.66H_2O$ and $SmPO_4 \cdot 0.66H_2O$ (based on earlier work by Mesbah et al. (2014) with which our results showed excellent agreement). The PXRD patterns were identical with a slight shift towards high angles resulting from decreasing ionic radius of lanthanides from La to Sm (Fig. 2).

In contrast, phosphate syntheses using solutions containing both Pb and LREE ions yielded crystalline precipitates with PXRD patterns very similar to each other (Fig. 3) but distinct from both $PbHPO_4$ and rhabdophanes. A slight shift in peak positions towards high angles resulting from different unit cell parameters of structures accommodating LREE with decreasing ionic radius was observed. This was identical to the shift observed for control rhabdophanes, indicating that La, Ce, Pr and Sm coprecipitated with Pb phosphates

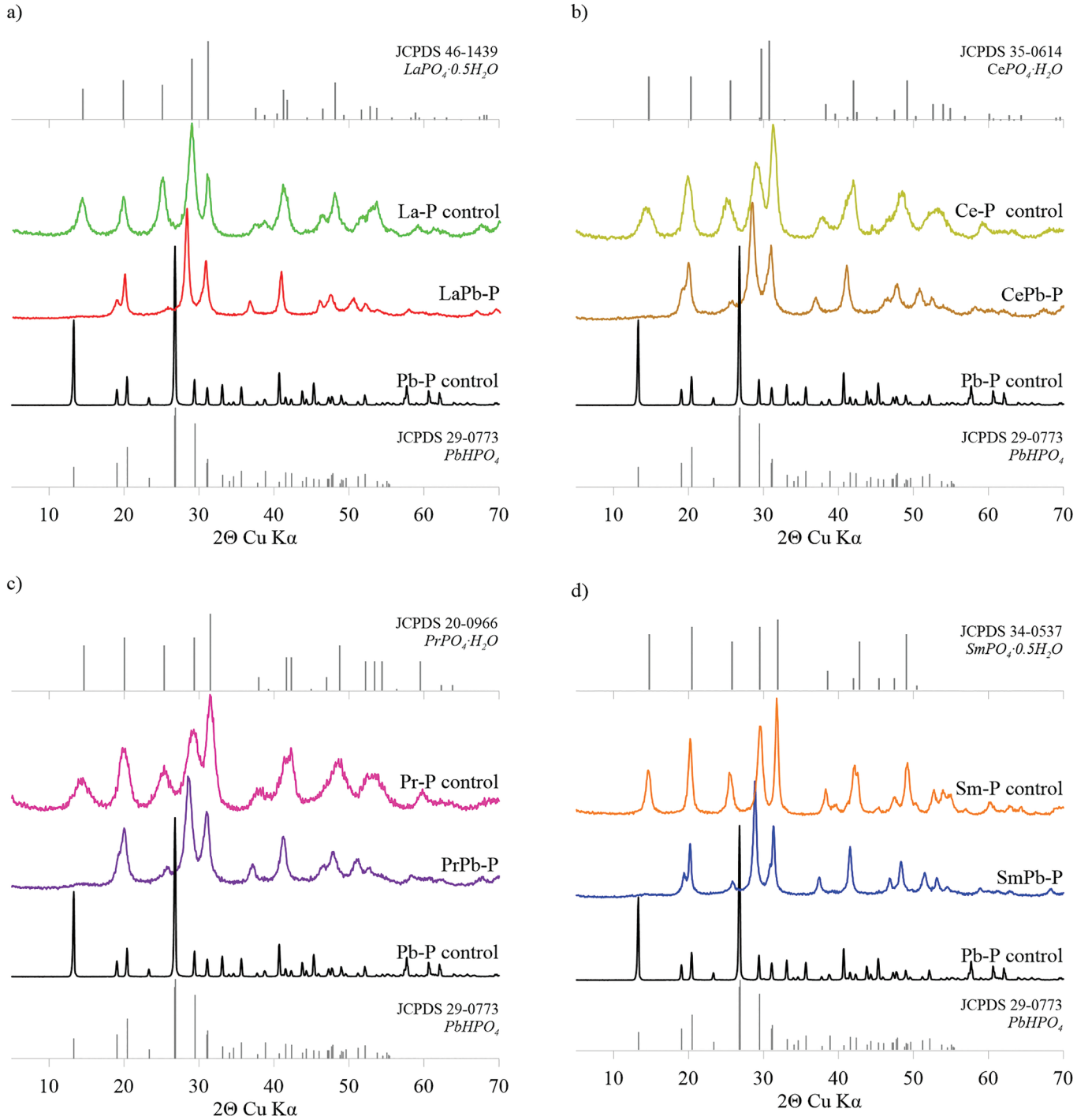


Figure 1. Comparison of PXRD patterns for products of the syntheses: a) LaPb-P and control samples (La-P and Pb-P); b) CePb-P and control samples (Ce-P and Pb-P); c) PrPb-P and control samples (Pr-P and Pb-P); d) SmPb-P and control samples (Sm-P and Pb-P). Samples with La or Sm were synthesized at pH=2 while samples containing Ce or Pr were synthesized at pH=3.

as analogous crystalline phases. The similarities and differences between the patterns are illustrated in Fig. 4 using La and Sm phosphates. The patterns of (LREE,Pb)-phosphates were very different from the patterns of control 'phosphoschultenite' indicating that this was not a REE-substituted $PbHPO_4$. They were also significantly different from other phases such as xenotime ($HREEPO_4$, tetragonal), monazite ($LREEPO_4$, monoclinic), or mixite group minerals (e.g., petersite $Cu_6Ce(PO_4)_3(OH)_6{\cdot}3H_2O$).

Despite the differences in the 10 – 30° 2Θ range, the diffraction patterns of (LREE,Pb)-phosphates show some resemblance to control rhabdophanes. Pb-containing rhabdophanes have been previously described by Walenta (2003). To explain the differences in PXRD patterns, Rietveld modelling of rhabdophanes with LREE partially substituted by Pb was attempted but did not give successful convergence (Fig. S1). This could be partly due to the poor crystallinity of the phases and the low quality of the PXRD data. The similarity of patterns between all four (LREE,Pb)-phosphates, however, indicates that the precipitate probably consists of a single phase, rather than a mixture of two phosphates. Indexing attempts by GSAS-II (Fig. S2) resulted in all cases in poor convergence at orthorhombic system, C*mmm* space group (Table 2). Unit cell parameters vary linearly with the ionic radius of LREE (Fig. S3) This needs to be confirmed in future by optimizing the synthesis

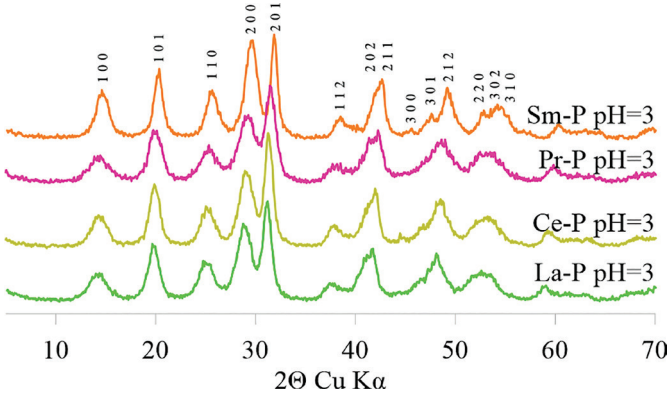


Figure 2. Comparison of PXRD patterns of (LREE)PO_4·0.66H_2O (LREE = La, Ce, Pr, Sm) synthesized at pH=3. Miller indices above peaks indicate structure identical with monoclinic rhabdophane. Slight shift of peak position results from decreasing ionic radius of lanthanides.

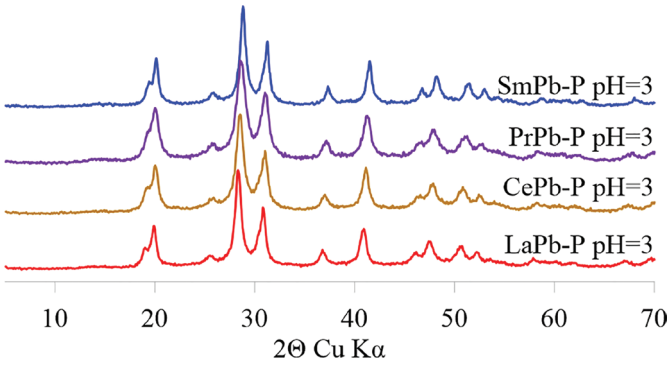


Figure 3. Comparison of PXRD patterns of (LREE,Pb)-phosphates synthesized at pH=3 indicating identical structure and shift resulting from decreasing ionic radius of lanthanides.

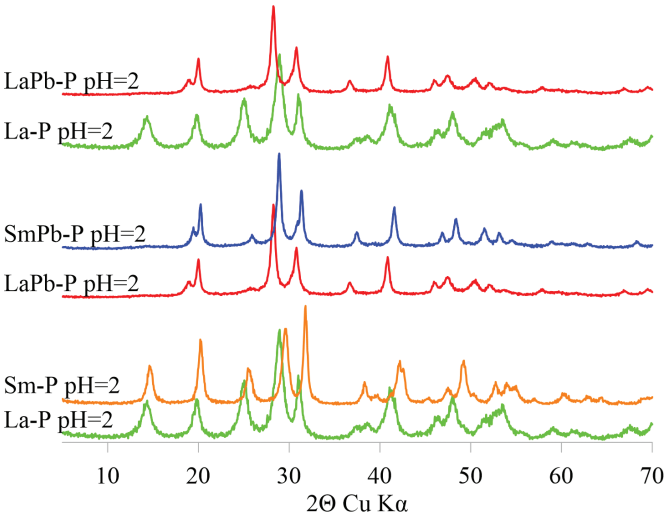


Figure 4. Superimposed diffraction patterns of selected synthesis products showing the differences or similarities of the structures of the resulting products and systematic shifts due to the different ionic radius of La and Sm.

Table 2. Calculated unit cell parameters of (LREE,Pb)-phosphates in orthorhombic system.

Phase	*a*	*b*	*c*	α = β = γ	*V*
	[Å]				[Å^3]
LaPb-P	4.62	5.76	7.01	90°	186.36
CePb-P	4.60	5.72	6.98		183.66
PrPb-P	4.56	4.68	6.94		179.80
SmPb-P	4.52	5.65	6.89		175.97

procedure to produce larger grains for single-crystal X-ray diffraction analysis.

To observe the possible effect of pH, the synthesis of La and Sm phosphates was repeated identically at pH 2, 3 and 4. No effect of pH was observed on the composition or structure of phosphates synthesized in the absence and presence of Pb at different pH. Comparison of diffraction patterns showed peak broadening with increasing pH which was particularly apparent at pH = 4 (Fig. 5). The feature is the most pronounced for rhabdophanes. This was partly due to the decreasing size of the crystallites with increased pH (consistent with the results of SEM imaging presented below), and partly due to the poor crystallinity associated with the higher degree of hydration (in accordance with the results of DTA/TG).

4.2. Morphology

SEM imaging confirmed the interpretation of the diffraction curves. All rhabdophanes crystallized in the similar form of 1-2 µm long circular needles (Fig. 6) similar to rhabdophanes reported in the literature (Gausse et al., 2016; Patra et al., 2005; Terra et al., 2003). Increasing pH resulted in the formation of smaller and more aggregated fibrous forms (Fig. S4) as previously reported by Sordyl et al. (2022) and in accordance with the broadened peaks on PXRD patterns. In contrast, phosphates containing LREE and Pb crystallized as needles in spherical aggregates (Fig. 7). The diameter of the aggregates was ~0.5 µm and decreased with increasing pH of the synthesis (Fig. S5).

4.3. Elemental composition

Elemental microanalysis of the La-P, Ce-P, Pr-P and Sm-P using SEM/EDS (Fig. S6, Table S1) revealed that the molar ratio of LREE:P was close to 1. This indicated the chemical formula: (LREE)PO_4·nH_2O consistent with rhabdophanes. The molar ratio of O:P increased at higher pH (for La and Sm phases), which may indicate the increasing hydration of the samples.

Wet chemical analysis of LaPb-P, CePb-P, PrPb-P and SmPb-P indicated that molar ratio of (LREE+Pb):P was between 1.27 and 1.38. The content of LREE with respect to Pb was somewhat higher for SmPb-P and PrPb-P (0.73 and 0.77, respectively) than for LaPb-P and CePb-P (0.68 and 0.65, respectively). Based on these results, calculated chemical formulas of newly discovered phases are: $La_2Pb_3(PO_4)_4$·nH_2O, $Ce_2Pb_3(PO_4)_4$·nH_2O, $Pr_2Pb_3(PO_4)_4$·nH_2O and $Sm_2Pb_3(PO_4)_4$·nH_2O. This way, the charges are balanced and molar ratios assumed in the chemical formula are close to these resulting from chemical analysis: (LREE+Pb):P equal to 1.25 and LREE:Pb equal to 0.67. This formula is different from natural phase $Pb(Ce,REE)_3(PO_4)_3(OH)_2$·n$H_2O$, known as UM2006-35-PO:HPbREEY, described by Plasil et al. (2009).

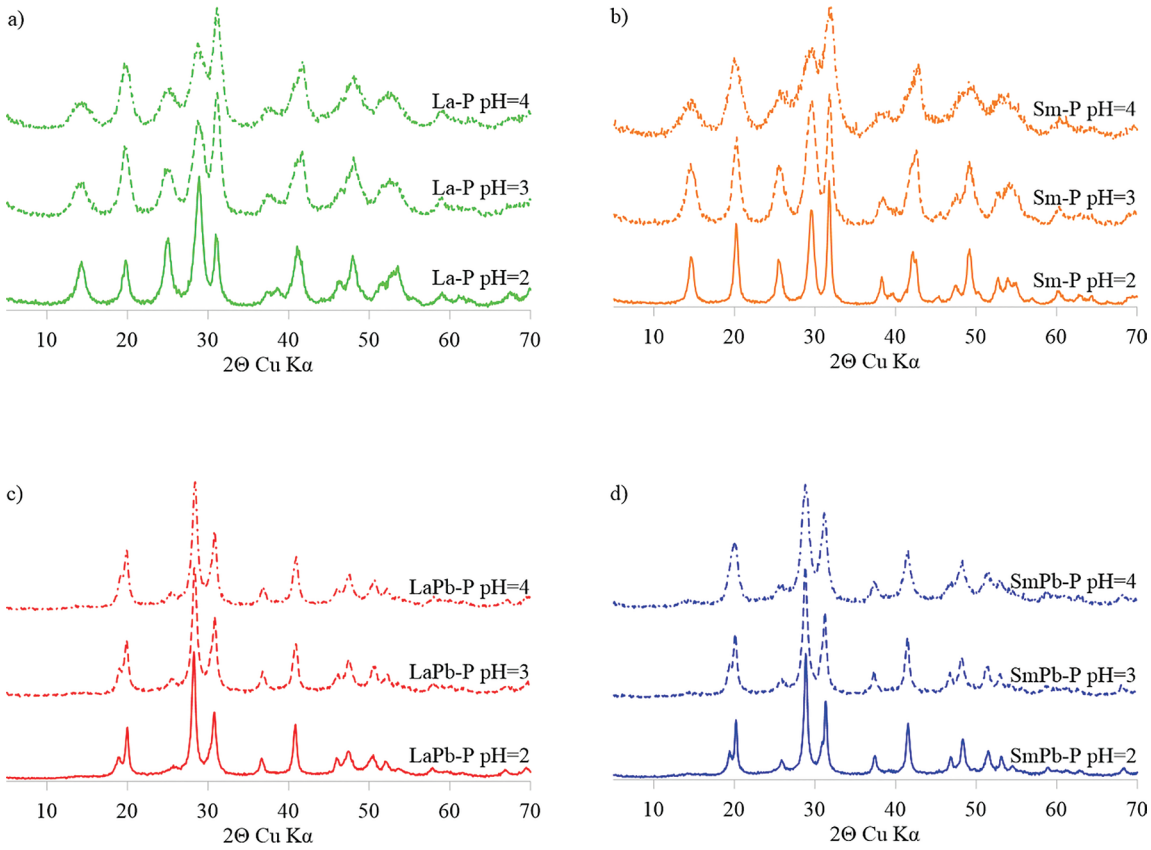


Figure 5. Comparison of diffraction patterns of La and Sm products synthesized at various pH, in the absence (a and b) or in the presence of Pb (c and d). Peak broadening with increasing pH is apparent in all cases.

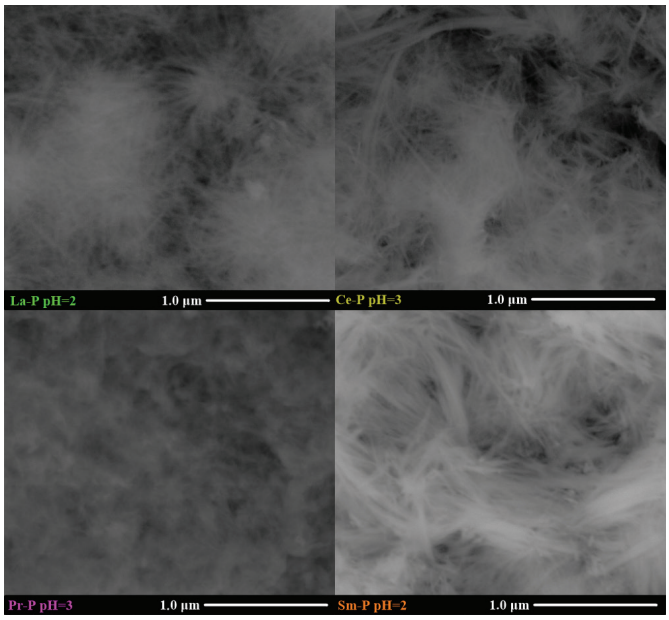


Figure 6. SEM (BSE) images of LREE-phosphates (rhabdophanes) synthesized at pH=2 or 3 in the absence of Pb.

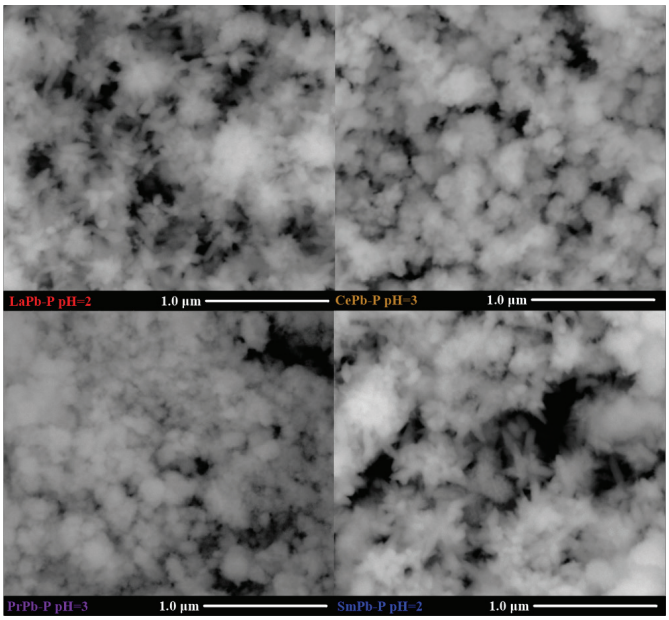


Figure 7. SEM (BSE) images of (LREE,Pb)-phosphates synthesized at pH=2 or 3 in the presence of Pb.

4.4. Structural features based on the FTIR

The IR spectrum of each phase is dominated by strong phosphate bands (broad, not fully resolved P-O v_1 symmetric and v_3 asymmetric stretching modes between 920 and 1070 cm^{-1}) and a broad band around 3455 cm^{-1} which was assigned to O-H stretching (v_1/v_3) modes in water molecules indicating that analyzed phases are hydrated (Fig. 8). The relatively small band apparent at around 1630 cm^{-1} was attributed to H-O-H bending (v_2) mode. All these phases are hydrated (Clavier et al., 2018). The relative intensity of these bands increased with the increase of pH indicating that phases precipitated at higher pH are more hydrated. However, no shift in position of bands was observed as a function of pH. Two or three bands, depending on the sample, around 540, 570 and 610 cm^{-1} were assigned to O-P-O v_4 asymmetric bending mode. Spectra of phases lacking Pb contained broad, low intensity band with maximum at around 2000 cm^{-1} that was attributed to series of overtones of phosphate group (Manecki et al., 2000). Those overtone bands were not present in the

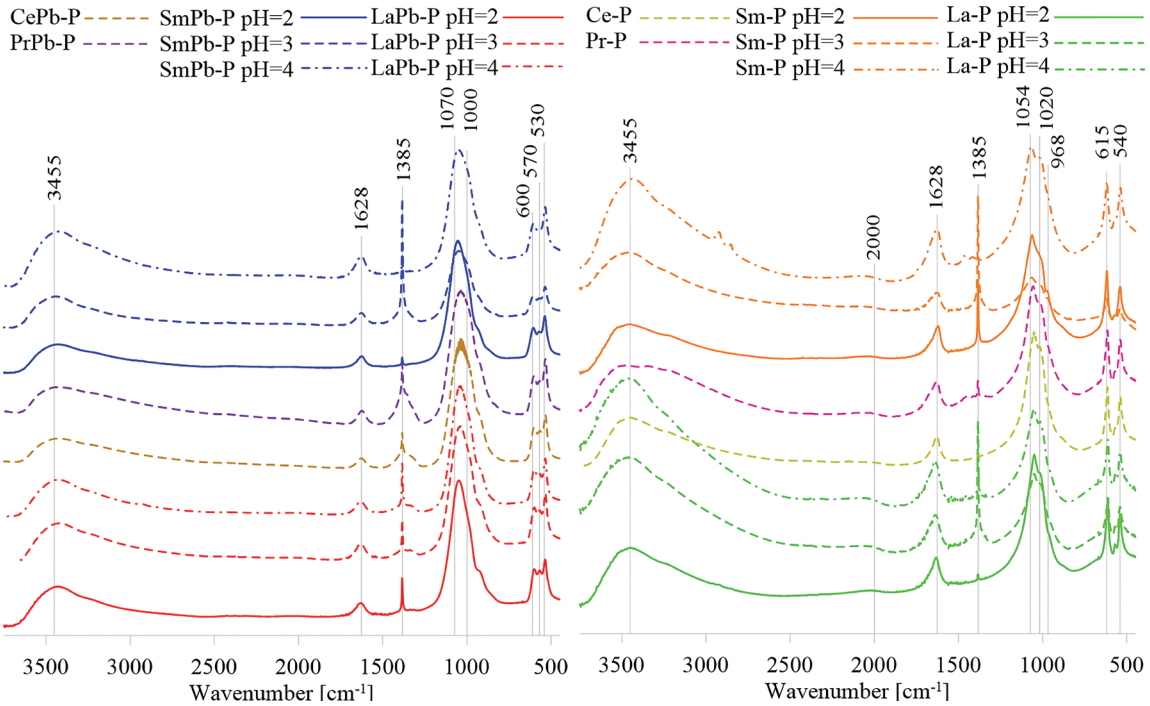


Figure 8. Comparison of FTIR spectra of LREE phosphates containing Pb (left) and Pb-free control phases (LREE rhabdophanes, right) precipitated at various pH.

spectra of phosphates containing Pb. This difference can be associated with high stability of Pb(II) – PO_4 bonds due to the presence of lone pair electrons (LEP) in coordination sphere of the Pb(II) by phosphate groups (Krivovichev, 2003). Also, splitting of two very intense bands (around 615 and 540 cm^{-1} for Pb-free phases) into three of lower intensity (around 600, 570 and 530 cm^{-1} for phosphates containing Pb) may suggest deformation of inner structure resulting from the presence of Pb ions. Small shift of the position of strong phosphate modes between 920 and 1070 in the phosphates containig Pb indicated partial substitution of Pb for LREE in the structure of these hydrated phosphates. The band at 1385 cm^{-1} was attributed to the NO_3^- group. Most likely it was the artifact of residual $NaNO_3$ that was not washed out completely after the synthesis (Diaz-Guillén et al., 2007). The spectra of control samples confirmed the formation of rhabdophanes (Diaz-Guillén et al., 2007; Heuser et al., 2014). The spectra of (LREE,Pb)-phosphates could not be assigned to any known mineral or synthetic phase.

4.5. Thermal stability and the degree of hydratation

The thermogram plots of (LREE,Pb)-phosphates and Pb-free controls are shown in Fig. 9 (TG, DTA and QMS, *m/z* = 18 – assigned as water vapor). The weight loss in two or three steps was observed similarly to the previously reported findings (Lucas et al., 2004). Temperature ranges of those steps were estimated based on DTA and QMS plots. For Pb-containing phases, the first two steps could not be precisely distinguished and were merged in one. The first step occurred below 200°C with an increase of intensity of the QMS plot and was associated with release of residual moisture adsorbed at the surface of the powders. The amount of adsorbed water varied between 3 and 10 wt% depending on crystal size affected by pH of the synthesis: the higher pH the smaller crystallites and the higher content of residual water. This varied mostly for control LREE rhabdophanes, while for (LREE,Pb)-phosphates variation of moisture content was minimal.

The second step occurred in the 170-300°C range and was most probably associated with the dehydration. The weight loss of 3-4 wt% was determined for control Pb-free phases. The lowest weight loss was observed for Ce-P at around 3.1 wt%. For phases containing Pb, cumulative weight loss during those two steps was on average between 4-5 wt%. Only SmPb-P synthesized at pH=4 showed weight loss around 8 wt% with a significant share below 200°C (possibly residual moisture). The lowest weight loss was observed for PrPb-P at around 4.1 wt%.

The third step occurred between 450 and 650°C and was accompanied by a water QMS signal with a maximum around 550-580°C. Based on the presence of O-H stretching band around 3455 cm^{-1} in FTIR spectra (Fig. 8), this increased QMS signal could be associated with dehydroxylation. In majority of analysed phases, no mass changes could be associated with this effect. Possible presence of hydroxyl groups is not certain but is negligible – the QMS signal and weight loss in this range were not as significant as in the first and second steps. Phases containing Ce and Pr did not exhibit increase in water QMS signal in this temperature range.

Endothermic effects present on DTA plots of phases containing Pb appeared above 850°C with varying temperatures of maximal intensities for each effect for different pH conditions during synthesis. For LaPb-P, the temperature of those effects increased with pH, while for SmPb-P temperature dropped. For CePb-P and PrPb-P those effects appeared near 1000°C. These effects appeared probably during phase transformations

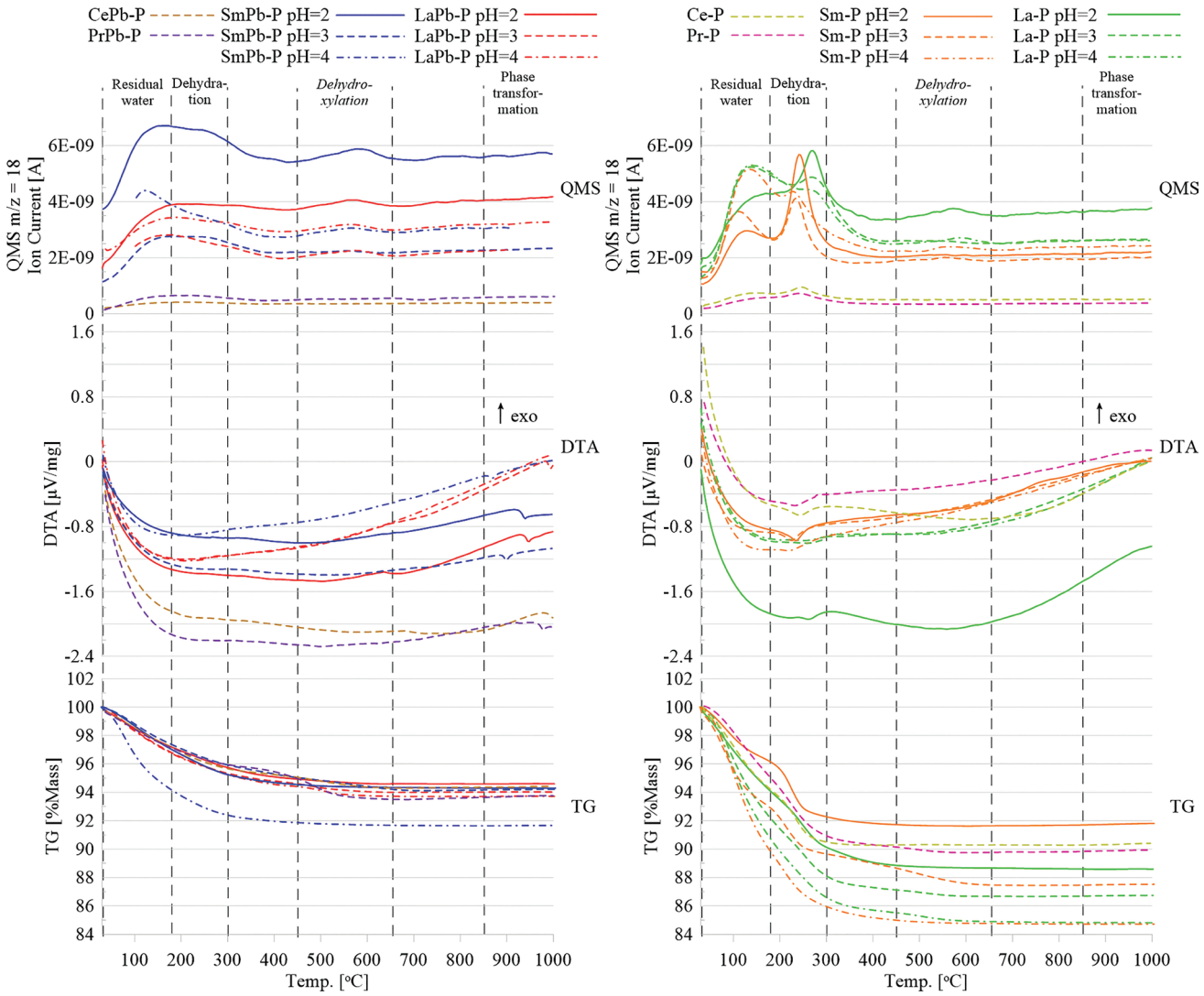


Figure 9. Comparison of TG, DTA and QMS *m/z* = 18 plots for Pb-rich (left) and Pb-free (right) LREE phosphates precipitated at various pH.

from the obtained (LREE)Pb-P phases to LREE oxides and anhydrous phosphates.

A total weight loss measured during the second step allows to determine the hydratation ratio *n* of analysed Pb-free control phosphates. The average *n* ratio is equal to 0.5 mole, resulting in the composition (LREE) $PO_4 \cdot 0.5H_2O$. Total cumulative weight loss in the first and second steps correspond to the *n* ratio of Pb-containing phases. The average *n* ratio is equal to 3.5 mole for LaPb-P, 3.3 mole for CePb-P, 3.1 mole for PrPb-P, and 3.3 mole for SmPb-P. Therefore, the calculated chemical formulas of newly discovered phases are $La_2Pb_3(PO_4)_4 \cdot 3.5H_2O$, $Ce_2Pb_3(PO_4)_4 \cdot 3.3H_2O$, $Pr_2Pb_3(PO_4)_4 \cdot 3.1H_2O$ and $Sm_2Pb_3(PO_4)_4 \cdot 3.3H_2O$. A trend can be seen in the general decreasing hydration ratio of REE-phosphates phases in the order from lighter to heavier REE. This is similar to previously reported Pb-free hydrous REE-phosphate phases (Shelyug et al., 2018).

5. Conclusions

Precipitation of LREE phosphates from aqueous solutions proceeded differently in the presence of Pb and resulted in formation of distinct hydrated phosphate phases containing both, Pb and LREE. Comparison with control phosphates indicates that these phases are not partially Pb-substituted rhabdophanes nor partially REE-substituted $PbHPO_4$. This showed that at the conditions of the experiment rhabdophane structures are reluctant to accept Pb substitutions and 'phosphoschultenite' structure did not accept isomorphic substitutions of LREE elements. The formation of a new, hitherto unknown crystalline phases was found which are mixed REE-Pb phosphates, orthorhombic in structure (*Cmmm* space group), with the composition $La_2Pb_3(PO_4)_4 \cdot 3.5H_2O$, $Ce_2Pb_3(PO_4)_4 \cdot 3.3H_2O$, $Pr_2Pb_3(PO_4)_4 \cdot 3.1H_2O$ and $Sm_2Pb_3(PO_4)_4 \cdot 3.3H_2O$. It is not certain whether similar mixed phosphates can also be formed with Heavy Rare Earth Elements (HREE). Our preliminary studies indicate that (HREE,Pb)-phosphates are not likely to form at this conditions (data not shown) while the potential effect of elevated temperature and/or pressure is unknown. The increase of pH from 2 to 4 affects only the morphology but not the composition of the precipitate. These phases were precipitated at experimental conditions similar to these used in a new coprecipitation route for the removal and recovery of REE from aqueous solutions (Sordyl et al., 2023). Optimization of the synthesis procedure will be necessary for full structural characteristics because of importance of these phases in technologies meeting the demand for REE. Formation of such phases may also be expected at various mineral waste landfills.

Declaration of Competing Interest

The authors declare that they have no known competing financial interests or personal relationships that could have appeared to influence the work reported in this paper.

Acknowledgments

We sincerely thank the Reviewers for their insightful and constructive observations. Theirs suggestions have been beneficial in improving the quality of our work.

This research was funded by program 'Excellence initiative – research university' for the AGH University of Krakow. JS was funded by Polish NCN research grant no. 2019/35/B/ST10/03379, KS was funded by Polish NCN research grant no. 2021/43/O/ST10/01282.

Supplementary Materials

Supplementary data to this article can be found online at https://doi.org/10.2478/mipo-2023-0006.

References

Achary, S. N., Bevara, S., & Tyagi, A. K. (2017). Recent progress on synthesis and structural aspects of rare-earth phosphates. *Coordination Chemistry Reviews*, *340*, 266–297. https://doi.org/10.1016/j.ccr.2017.03.006

Alonso, E., Sherman, A. M., Wallington, T. J., Everson, M. P., Field, F. R., Roth, R., & Kirchain, R. E. (2012). Evaluating Rare Earth Element Availability: A Case with Revolutionary Demand from Clean Technologies. *Environmental Science & Technology*, *46*(6), 3406–3414. https://doi.org/10.1021/es203518d

Ang, K. L., Li, D., & Nikoloski, A. N. (2017). The effectiveness of ion exchange resins in separating uranium and thorium from rare earth elements in acidic aqueous sulfate media. Part 1. Anionic and cationic resins. *Hydrometallurgy*, *174*, 147–155. https://doi.org/10.1016/j.hydromet.2017.10.011

Apergis, E., & Apergis, N. (2017). *The role of rare earth prices in renewable energy consumption: The actual driver for a renewable energy world | Energy Economics, 62*, 33-42. https://doi.org/10.1016/j.eneco.2016.12.015

Balaram, V. (2019). Rare earth elements: A review of applications, occurrence, exploration, analysis, recycling, and environmental impact. *Geoscience Frontiers*, *10*(4), 1285–1303. https://doi.org/10.1016/j.gsf.2018.12.005

Belardi, G., Ippolito, N., Piga, L., & Serracino, M. (2014). Investigation on the status of rare earth elements contained in the powder of spent fluorescent lamps. *Thermochimica Acta*, *591*, 22–30. https://doi.org/10.1016/j.tca.2014.07.015

Berger, A., Gnos, E., Janots, E., Fernandez, A., & Giese, J. (2008). Formation and composition of rhabdophane, bastnäsite and hydrated thorium minerals during alteration: Implications for geochronology and low-temperature processes. *Chemical Geology*, *254*(3–4), 238–248. https://doi.org/10.1016/j.chemgeo.2008.03.006

Binnemans, K., Jones, P. T., Blanpain, B., Van Gerven, T., & Pontikes, Y. (2015). Towards zero-waste valorisation of rare-earth-containing industrial process residues: A critical review. *Journal of Cleaner Production*, *99*, 17–38. https://doi.org/10.1016/j.jclepro.2015.02.089

Binnemans, K., Jones, P. T., Blanpain, B., Van Gerven, T., Yang, Y., Walton, A., & Buchert, M. (2013). Recycling of rare earths: A critical review. *Journal of Cleaner Production*, *51*, 1–22. https://doi.org/10.1016/j.jclepro.2012.12.037

Cánovas, C. R., Chapron, S., Arrachart, G., & Pellet-Rostaing, S. (2019). Leaching of rare earth elements (REEs) and impurities from phosphogypsum: A preliminary insight for further recovery of critical raw materials. *Journal of Cleaner Production*, *219*, 225–235. https://doi.org/10.1016/j.jclepro.2019.02.104

Cánovas, C. R., Pérez-López, R., Macías, F., Chapron, S., Nieto, J. M., & Pellet-Rostaing, S. (2017). Exploration of fertilizer industry wastes as potential source of critical raw materials. *Journal of Cleaner Production*, *143*, 497–505.https://doi.org/10.1016/j.jclepro.2016.12.083

Clavier, N., Mesbah, A., Szenknect, S., & Dacheux, N. (2018). Monazite, rhabdophane, xenotime & churchite: Vibrational spectroscopy of gadolinium phosphate polymorphs. *Spectrochimica Acta Part A: Molecular and Biomolecular Spectroscopy*, *205*, 85–94. https://doi.org/10.1016/j.saa.2018.07.016

Das, S., Gaustad, G., Sekar, A., & Williams, E. (2018). Techno-economic analysis of supercritical extraction of rare earth elements from coal ash. *Journal of Cleaner Production*, *189*, 539–551. https://doi.org/10.1016/j.jclepro.2018.03.252

Diaz-Guillén, J. A., Fuentes, A. F., Gallini, S., & Colomer, M. T. (2007). A rapid method to obtain nanometric particles of rhabdophane $LaPO_4{\cdot}nH_2O$ by mechanical milling. *Journal of Alloys and Compounds*, *427*(1–2), 87–93. https://doi.org/10.1016/j.jallcom.2006.03.011

Emsbo, P., McLaughlin, P. I., Breit, G. N., du Bray, E. A., & Koenig, A. E. (2015). Rare earth elements in sedimentary phosphate deposits: Solution to the global REE crisis? *Gondwana Research*, *27*(2), 776–785. https://doi.org/10.1016/j.gr.2014.10.008

Gausse, C., Szenknect, S., Qin, D. W., Mesbah, A., Clavier, N., Neumeier, S., Bosbach, D., & Dacheux, N. (2016). Determination of the Solubility of Rhabdophanes $LnPO_4{\cdot}0.667H_2O$ (Ln = La to Dy). *European Journal of Inorganic Chemistry*, *2016*(28), 4615–4630. https://doi.org/10.1002/ejic.201600517

Gelcich, S., Davis, D. W., & Spooner, E. T. C. (2005). Testing the apatite-magnetite geochronometer: U-Pb and $^{40}Ar/^{39}Ar$ geochronology of plutonic rocks, massive magnetite-apatite tabular bodies, and IOCG mineralization in Northern Chile. *Geochimica et Cosmochimica Acta*, *69*(13), 3367–3384. https://doi.org/10.1016/j.gca.2004.12.020

He, Y., Guo, S., Chen, K., Li, S., Zhang, L., & Yin, S. (2019). Sustainable Green Production: A Review of Recent Development on Rare Earths Extraction and Separation

Using Microreactors. *ACS Sustainable Chemistry & Engineering*, *7*(21), 17616–17626. https://doi.org/10.1021/acssuschemeng.9b03384

Hermassi, M., Granados, M., Valderrama, C., Ayora, C., & Cortina, J. L. (2021). Recovery of Rare Earth Elements from acidic mine waters by integration of a selective chelating ion-exchanger and a solvent impregnated resin. *Journal of Environmental Chemical Engineering*, *9*(5), 105906. https://doi.org/10.1016/j.jece.2021.105906

Heuser, J., Bukaemskiy, A. A., Neumeier, S., Neumann, A., & Bosbach, D. (2014). Raman and infrared spectroscopy of monazite-type ceramics used for nuclear waste conditioning. *Progress in Nuclear Energy*, *72*, 149–155. https://doi.org/10.1016/j.pnucene.2013.09.003

Hossain, M. K., Rubel, M. H. K., Akbar, M. A., Ahmed, M. H., Haque, N., Rahman, Md. F., Hossain, J., & Hossain, K. M. (2022). A review on recent applications and future prospects of rare earth oxides in corrosion and thermal barrier coatings, catalysts, tribological, and environmental sectors. *Ceramics International*, *48*(22), 32588–32612. https://doi.org/10.1016/j.ceramint.2022.07.220

Innocenzi, V., De Michelis, I., Kopacek, B., & Vegliò, F. (2014). Yttrium recovery from primary and secondary sources: A review of main hydrometallurgical processes. *Waste Management*, *34*(7), 1237–1250. https://doi.org/10.1016/j.wasman.2014.02.010

Kifle, D., & Wibetoe, G. (2013). Selective liquid chromatographic separation of yttrium from heavier rare earth elements using acetic acid as a novel eluent. *Journal of Chromatography A*, *1307*, 86–90. https://doi.org/10.1016/j.chroma.2013.07.070

Krivovichev, S. V. (2003, April 6). *Structural chemistry of basic Pb(II) oxysalt minerals and inorganic compounds*. EGS - AGU - EUG Joint Assembly, Nice, France.

Kulczycka, J., Kowalski, Z., Smol, M., & Wirth, H. (2016). Evaluation of the recovery of Rare Earth Elements (REE) from phosphogypsum waste – case study of the WIZÓW Chemical Plant (Poland). *Journal of Cleaner Production*, *113*, 345–354. https://doi.org/10.1016/j.jclepro.2015.11.039

Kumari, A., Dipali, Randhawa, N. S., & Sahu, S. K. (2021). Electrochemical treatment of spent NdFeB magnet in organic acid for recovery of rare earths and other metal values. *Journal of Cleaner Production*, *309*, 127393. https://doi.org/10.1016/j.jclepro.2021.127393

Laatikainen, M., Makarova, I., Sainio, T., & Repo, E. (2021). Selective acid leaching of rare earth elements from roasted NdFeB magnets. *Separation and Purification Technology*, *278*, 119571. https://doi.org/10.1016/j.seppur.2021.119571

Li, Q., Ji, B., Honaker, R., Noble, A., & Zhang, W. (2022). Partitioning behavior and mechanisms of rare earth elements during precipitation in acid mine drainage. *Colloids and Surfaces A: Physicochemical and Engineering Aspects*, *641*, 128563. https://doi.org/10.1016/j.colsurfa.2022.128563

Lucas, S., Champion, E., Bernache-Assollant, D., & Leroy, G. (2004). Rare earth phosphate powders $RePO_4 \cdot nH_2O$ (Re=La, Ce or Y) II. Thermal behavior. *Journal of Solid State Chemistry*, *177*(4–5), 1312–1320. https://doi.org/10.1016/j.jssc.2003.11.004

Makarova, I., Soboleva, E., Osipenko, M., Kurilo, I., Laatikainen, M., & Repo, E. (2020). Electrochemical leaching of rare-earth elements from spent NdFeB magnets. *Hydrometallurgy*, *192*, 105264. https://doi.org/10.1016/j.hydromet.2020.105264

Mancheri, N. A., Sprecher, B., Bailey, G., Ge, J., & Tukker, A. (2019). Effect of Chinese policies on rare earth supply chain resilience. *Resources, Conservation and Recycling*, *142*, 101–112. https://doi.org/10.1016/j.resconrec.2018.11.017

Manecki, M., Maurice, P. A., & Traina, S. J. (2000). Uptake of aqueous Pb by Cl^- , F^- , and OH^- apatites: Mineralogic evidence for nucleation mechanisms. *American Mineralogist*, *85*(7–8), 932–942. https://doi.org/10.2138/am-2000-0707

Max-Hansen, M., Ojala, F., Kifle, D., Borg, N., & Nilsson, B. (2011). Optimization of preparative chromatographic separation of multiple rare earth elements. *Journal of Chromatography A*, *1218*(51), 9155–9161. https://doi.org/10.1016/j.chroma.2011.10.062

Mesbah, A., Clavier, N., Elkaim, E., Gausse, C., Kacem, I. B., Szenknect, S., & Dacheux, N. (2014). Monoclinic Form of the Rhabdophane Compounds: $REEPO_4 \cdot 0.667H_2O$. *Crystal Growth & Design*, *14*(10), 5090–5098. https://doi.org/10.1021/cg500707b

Mesbah, A., Clavier, N., Elkaim, E., Szenknect, S., & Dacheux, N. (2017). In pursuit of the rhabdophane crystal structure: From the hydrated monoclinic $LnPO_4.0.667H_2O$ to the hexagonal $LnPO_4$ (Ln = Nd, Sm, Gd, Eu and Dy). *Journal of Solid State Chemistry*, *249*, 221–227. https://doi.org/10.1016/j.jssc.2017.03.004

Młynarska, M., Manecki, M., & Bajda, T. (2014). Structural and Raman spectroscopy studies of schultenite—Phosphoschultenite isomorphic series. *Geology, Geophysics and Environment*, *Vol. 40*(1). http://yadda.icm.edu.pl/baztech/element/bwmeta1.element.baztech-aeb77a41-84f3-473c-aa68-105bf3118a49

Müller, M. A., Schweizer, D., & Seiler, V. (2016). Wealth Effects of Rare Earth Prices and China's Rare Earth Elements Policy. *Journal of Business Ethics*, *138*(4), 627–648. https://doi.org/10.1007/s10551-015-2773-3

Patra, C. R., Alexandra, G., Patra, S., Jacob, D. S., Gedanken, A., Landau, A., & Gofer, Y. (2005). Microwave approach for the synthesis of rhabdophane-type lanthanide orthophosphate (Ln = La, Ce, Nd, Sm, Eu, Gd and Tb) nanorods under solvothermal conditions. *New Journal of Chemistry*, *29*(5), 733. https://doi.org/10.1039/b415693e

Plášil, J., Sejkora, J., Čejka, J., Škoda, R., & Goliáš, V. (2009). Supergene mineralization of the Medvedin uranium deposit, Krkonose Mountains, Czech Republic. *Journal of Geosciences*, *54*(1), 15–56. https://doi.org/10.3190/jgeosci.029

Proelss, J., Schweizer, D., & Seiler, V. (2020). *The economic importance of rare earth elements volatility forecasts | International Review of Financial Analysis, 71,* 101316. https://doi.org/10.1016/j.irfa.2019.01.010

Pyrzynska, K., Kubiak, A., & Wysocka, I. (2016). Application of solid phase extraction procedures for rare earth

elements determination in environmental samples. *Talanta*, *154*, 15–22. https://doi.org/10.1016/j.talanta.2016.03.022

Rafiuddin, M. R., Tyagi, C., & Haq, M. A. (2022). Synthesis and structural investigation of churchite-type $REPO_4 \cdot 2H_2O$ (RE = Y, Gd, Dy) nanocrystals. *Journal of Solid State Chemistry*, *311*, 123150. https://doi.org/10.1016/j.jssc.2022.123150

Rychkov, V. N., Kirillov, E. V., Kirillov, S. V., Semenishchev, V. S., Bunkov, G. M., Botalov, M. S., Smyshlyaev, D. V., & Malyshev, A. S. (2018). Recovery of rare earth elements from phosphogypsum. *Journal of Cleaner Production*, *196*, 674–681. https://doi.org/10.1016/j.jclepro.2018.06.114

Sengupta, P. (2012). A review on immobilization of phosphate containing high level nuclear wastes within glass matrix – Present status and future challenges. *Journal of Hazardous Materials*, *235–236*, 17–28. https://doi.org/10.1016/j.jhazmat.2012.07.039

Shelyug, A., Mesbah, A., Szenknect, S., Clavier, N., Dacheux, N., & Navrotsky, A. (2018). Thermodynamics and Stability of Rhabdophanes, Hydrated Rare Earth Phosphates $REPO_4 \cdot nH_2O$. *Frontiers in Chemistry*, *6*, 604. https://doi.org/10.3389/fchem.2018.00604

Shimizu, R., Sawada, K., Enokida, Y., & Yamamoto, I. (2005). Supercritical fluid extraction of rare earth elements from luminescent material in waste fluorescent lamps. *The Journal of Supercritical Fluids*, *33*(3), 235–241. https://doi.org/10.1016/j.supflu.2004.08.004

Shinde, K. N., & Dhoble, S. J. (2014). Europium-Activated Orthophosphate Phosphors For Energy-Efficient Solid-State Lighting: A Review. *Critical Reviews in Solid State and Materials Sciences*, *39*(6), 459–479. https://doi.org/10.1080/10408436.2013.803456

Sordyl, J., Majka, J., Högdahl, K., & Manecki, M. (2023, 29.08). *Rare earth elements recovery from apatite*. SEG 2023 Conference: Resourcing the Green Transition.

Sordyl, J., Rybka, K., Dziewiątka, K., Jędras, A., Skalny, M., Staszel, K., Tomczak, A., Urbański, K., & Manecki, M. (2022, May 23). *The influence of the synthesis procedure on the morphology of REE-enriched Pb-apatite (pyromorphite)*. EGU General Assembly 2022, Vienna, Austria. https://doi.org/10.5194/egusphere-egu22-7905

Strzelecki, A. C., Reece, M., Zhao, X., Yu, W., Benmore, C., Ren, Y., Alcorn, C., Migdisov, A., Xu, H., & Guo, X. (2022). Crystal Chemistry and Thermodynamics of HREE (Er, Yb) Mixing in a Xenotime Solid Solution. *ACS Earth and Space Chemistry*, *6*(5), 1375–1389. https://doi.org/10.1021/acsearthspacechem.2c00052

Subramani, T., Rafiuddin, M. R., Shelyug, A., Ushakov, S., Mesbah, A., Clavier, N., Qin, D., Szenknect, S., Elkaim, E., Dacheux, N., & Navrotsky, A. (2019). Synthesis, Crystal Structure, and Enthalpies of Formation of Churchite-type $REPO_4 \cdot 2H_2O$ (RE = Gd to Lu) Materials. *Crystal Growth & Design*, *19*(8), 4641–4649. https://doi.org/10.1021/acs.cgd.9b00524

Talan, D., & Huang, Q. (2022). A review of environmental aspect of rare earth element extraction processes and solution purification techniques. *Minerals Engineering*, *179*, 107430. https://doi.org/10.1016/j.mineng.2022.107430

Terra, O., Clavier, N., Dacheux, N., & Podor, R. (2003). Preparation and characterization of lanthanum–gadolinium monazites as ceramics for radioactive waste storage. *New J. Chem.*, *27*(6), 957–967. https://doi.org/10.1039/B212805P

Traore, M., Gong, A., Wang, Y., Qiu, L., Bai, Y., Zhao, W., Liu, Y., Chen, Y., Liu, Y., Wu, H., Li, S., & You, Y. (2022). Research progress of rare earth separation methods and technologies. *Journal of Rare Earths*, S1002072122001065. https://doi.org/10.1016/j.jre.2022.04.009

Vaziri Hassas, B., Shekarian, Y., & Rezaee, M. (2023). Selective precipitation of rare earth and critical elements from acid mine drainage - Part I: Kinetics and thermodynamics of staged precipitation process. *Resources, Conservation and Recycling*, *188*, 106654. https://doi.org/10.1016/j.resconrec.2022.106654

Walenta, K. (2003). Monokliner bleihaltiger Rhabdophan von der Grube Clara im mittleren Schwarzwald. *Aufschluss*, *54*, 405–409.

Wudarska, A., Sordyl, J., Manecki, M., Zawiła, A., & Bajda, T. (2022). Vibrational spectroscopic study of synthetic analogs of schultenite PbHAsO4–"phosphoschultenite" $PbHPO_4$ solid solution series. *Polyhedron*, *211*, 115534. https://doi.org/10.1016/j.poly.2021.115534

Zhang, Y., Gao, Y., Wang, P., Na, D., Yang, Z., & Zhang, J. (2022). Solvent extraction of Ce(III) and Pr(III) with P507 using SiC foam as a static mixer. *Journal of Rare Earths*, *40*(4), 676–686. https://doi.org/10.1016/j.jre.2021.02.002

Received: 30 May 2023
Accepted: 13 Nov 2023
Handling Editor: Jaroslaw Majka